Proceedings of ICMM2005
3rd International Conference on Microchannels and Minichannels
June 13-15, 2005, Toronto, Ontario, Canada

ICMM2005-75141

MODELING AND DESIGN OF MICRO-GROOVED FLAT PLATE EVAPORATOR

Naoki Shikazono[1], Yasushi Suehisa[1], Nobuhide Kasagi[1] and Hiroshi Iwata[2]

[1]The University of Tokyo, 7-3-1 Hongo, Bunkyo-ku, Tokyo, Japan
[2]Nichirei Industries Co. Ltd., 1570 Mayumi, Ohhira-machi, Tochigi-ken, Japan

ABSTRACT

A micro-grooved flat plate evaporator is modeled and its heat transfer characteristics are investigated numerically and experimentally. A test model is developed for the vapor compression cycle evaporator, where pressure gradient drives the vapor and the liquid flow. In this study, the effect of pressure gradient is implicitly introduced through the Smith's equation for predicting void fraction from given quality. The film thickness profile in the micro region near the contact line is obtained by solving the 4th order differential equation. Then the local heat flux is obtained by assuming that the heat conduction through the liquid is one dimensional in the wall normal direction. The shape of liquid-vapor interface is assumed to be a circular arc in the macro region, whose radius is directly linked to the void fraction. This curvature radius is used as the boundary condition for the micro region model at the micro-macro interface.

Finally, the heat transfer coefficient on a micro-grooved flat plate evaporator is measured in a HFC134a experimental loop and compared with the numerical prediction. The present model assumptions are validated and assessed.

Keywords: Evaporator, Micro-Groove, Thin Film, Surface Tension, Disjoining Pressure.

INTRODUCTION

Since thin liquid films can promote very rapid and intensive heat and mass transfer, micro-grooved surfaces have been attracting large attention in the area of refrigeration and air conditioning industries. In fact, micro-fin tubes are recognized as one of the most successful heat transfer enhancement technologies. On the other hand, for the temperature control of electronic or biotechnology applications, it is common that the heat has to be removed from one side of the device. Thus, flat plate evaporators are considered to be an important technology for such applications. In case of micro-grooved evaporators, it is known that intensive evaporation can be achieved in a region near the contact line where very thin liquid films are formed adjacent to the adsorbed film region (see, e.g. Wayner [1,2]). However, this strong evaporation occurs at a very limited area only in the vicinity of the contact line. Thus, the main challenge in developing an efficient evaporator is to spotlight such microscopic strong evaporation region on a macroscopic heat transfer surface. It is expected that numerical simulation can be a powerful design tool for this purpose.

In the present study, a micro-grooved flat plate evaporator is simulated analytically extending the method proposed by previous researchers, e.g. Wayner, et al. [3,4], Kamotani [5] and Stephan and Busse[6] etc. In the following sections, the model equations for the micro and macro regions are presented. Finally, the model is compared with the experimental results and the model assumptions are validated and assessed.

NOMENCLATURE

A	dispersion constant, J or area, m^2
f	accommodation coefficient, dimensionless
G	macro region mass flow rate, kg/s
g	macro region evaporation rate per unit length, kg/(m·s)
h	channel height, m
h_{fg}	specific heat of evaporation, J/kg
K	curvature of the meniscus, 1/m
M	micro region mass flow rate, kg/s
m	micro region evaporation rate per unit length, kg/(m·s)
p	pressure, Pa
q	heat flux, W/m^2
Q	heat transfer, W
R	curvature radius, m

R_g gas constant, J/(kg·K)
$S(x)$ wet area width at position x, m
T temperature, K
w groove width, m
x coordinate along the groove, m
z transformed variable for solving Eq. (10)
α heat transfer coefficient, W/(m^2·K)
β void fraction, dimensionless
δ film thickness, m
γ groove angle, rad
η viscosity, Pa·s
λ thermal conductivity, W/(m·K)
ν kinematic viscosity, m^2/s
ρ density, kg/m^3
σ surface tension, N/m
ξ flow direction in the micro region, m
ζ distance from the wall, m

SUBSCRIPT

c capillary
end end boundary
iv vapor side of the liquid-vapor interface
in inlet boundary
l liquid
m mean
s solid
sat saturation
v vapor

MODELING OF A FLAT PLATE EVAPORATOR

Figure 1 shows the cross section of the micro-grooved flat plate evaporator. Heat is removed from one side of the wall. The flow inside the groove is divided into two regions, i.e., micro and macro regions. These two regions are modeled individually as is commonly done for solving thin film evaporation. Following the method proposed by previous researchers, e.g. Wayner, et al. [3,4], Kamotani [5] and Stephan and Busse[6] etc., a differential equation of the liquid film thickness is solved for the micro region. On the other hand, very simple heat conduction equations have been applied for calculations of the macro region. This approximation is thought to be acceptable because local heat flux in the macro region is an order of magnitude smaller than that in the micro region. The liquid film thickness, film inclination angle and

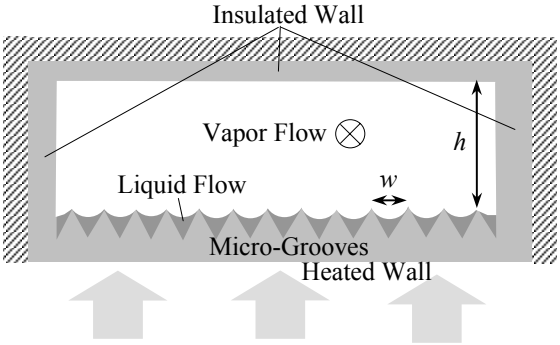

Fig. 1 Cross section of the micro-grooved flat plate evaporator

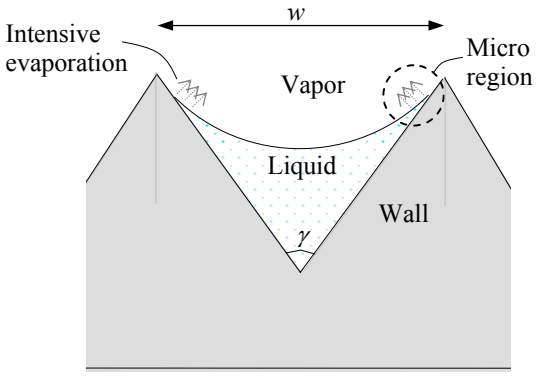

Fig. 2 Meniscus of liquid in a triangular groove

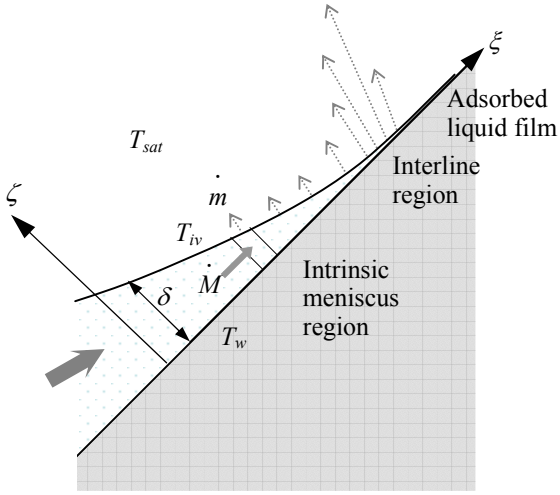

Fig. 3 Enlarged view of the micro region

curvature are connected smoothly at the boundary. Ajaev and Homsy [7] combined these two regions using asymptotic matching. In the present study, the micro and macro regions are simply combined at the position at the limit where the total heat transfer rate is not affected by its location. In the following sections, the models for micro and macro regions are described.

Micro Region Model

Following previous study of a falling film evaporator (Hasebe et. al. [8]), the analytical model described by Stephan and Busse [6] is adopted for the micro region. Since the liquid film is very thin and the surface tension becomes dominant in this scale, gravitational effects are ignored in the micro model. Figure 2 shows the meniscus of the liquid captured in a triangular groove, and Fig. 3 shows the enlarged view of the micro region. In this study, triangular shape is adopted for the cross section of the groove because of the simplicity of analytical treatment.

Intensive evaporation takes place at the so-called interline region where the liquid film gets very thin. The heat flux $\dot{q}$ in the liquid film is assumed to be one dimensional in the wall normal direction and can be written as

$$\dot{q} = \frac{T_W - T_{sat}\left(1 + \dfrac{p_c}{h_{fg}\rho_l}\right)}{\dfrac{\delta}{\lambda_l} + \dfrac{T_{sat}\sqrt{(2\pi R_g T_{sat})}}{h_{fg}^2 \rho_v}\dfrac{(2-f)}{2f}}, \quad (1)$$

where the first and the second terms in the denominator correspond to the heat conduction resistance and interfacial heat resistance, respectively. Constant wall temperature T_w is assumed in this study. The effect of wall conductivity is reported to be less than 15 % in case of aluminum groove with heat flux of 30 kW/m^2 [6]. Thus, constant wall temperature assumption seems reasonable for cupper wall with moderate heat flux. The accommodation coefficient f expresses the fraction of molecules actually vaporized at the surface (the remaining 1-f is due to the reflection of vapor molecules). In the present study, $f = 1$ is used unless otherwise noted. The pressure difference between vapor and liquid phases p_c is expressed as

$$p_c = p_v - p_l = K\sigma + \frac{A}{\delta^3}. \quad (2)$$

The first and the second terms describe the surface tension and the disjoining pressure effects, respectively. The dispersion constant was set as $A = 2.0 \times 10^{-21}$ J [6]. The curvature K can be expressed using the film thickness δ as

$$K = \frac{\dfrac{d^2\delta}{d\xi^2}}{\left\{1 + \left(\dfrac{d\delta}{d\xi}\right)^2\right\}^{3/2}}. \quad (3)$$

This pressure gradient due to the film thickness profile pulls the liquid to the strong evaporating interline region and balances with the viscous drag of the flow.

The local and mean velocity profiles u and $\bar{u}$ in a laminar boundary layer are given as

$$u = \frac{1}{\mu}\frac{dp_l}{d\xi}\left(\frac{\zeta^2}{2} - \delta\zeta\right), \quad (4)$$

$$\bar{u} = \frac{1}{\delta}\int_0^\delta u d\zeta = -\frac{\delta^2}{3\nu_l\rho_l}\frac{dp_l}{d\xi}. \quad (5)$$

Then the mass flow rate $\dot{M}$ $(= \bar{u}\delta\rho_l)$ can be obtained using Eq. (5);

$$\dot{M} = -\frac{\delta^3}{3\nu_l}\frac{dp_l}{d\xi}. \quad (6)$$

Thus, the evaporation rate $\dot{m}$ is obtained as follows:

$$\dot{m} = -\frac{d\dot{M}}{d\xi} = \frac{1}{3\nu_l}\frac{d}{d\xi}\left(\delta^3\frac{dp_l}{d\xi}\right). \quad (7)$$

Assuming the vapor pressure p_v to be constant, the liquid phase pressure gradient is related to the capillary pressure gradient as

$$\frac{dp_l}{d\xi} = -\frac{dp_c}{d\xi}. \quad (8)$$

Thus, one obtains the expression for the heat flux as

$$\dot{q} = -\frac{h_{fg}}{3\nu_l}\frac{d}{d\xi}\left(\delta^3\frac{dp_c}{d\xi}\right). \quad (9)$$

Combining Eqs. (1), (2), (3) and (9), the fourth order differential equation for the liquid thickness δ is obtained;

$$\frac{\sigma}{3\mu_l}\frac{d}{d\xi}\left\{\delta^3\frac{d}{d\xi}\left(\frac{\dfrac{d^2\delta}{d\xi^2}}{\left\{1+\left(\dfrac{d\delta}{d\xi}\right)^2\right\}^{3/2}} + \frac{A}{\sigma\delta^3}\right)\right\} = \frac{T_{sat} - T_w + \dfrac{T_{sat}\sigma}{h_{fg}\rho_l}\left[\dfrac{\dfrac{d^2\delta}{d\xi^2}}{\left\{1+\left(\dfrac{d\delta}{d\xi}\right)^2\right\}^{3/2}} + \dfrac{A}{\sigma\delta^3}\right]}{\rho_l h_{fg}\left(\dfrac{\delta}{\lambda_l} + \dfrac{T_{sat}\sqrt{2\pi R_g T_{sat}}}{h_{fg}^2\rho_v}\dfrac{2-f}{2f}\right)}. \quad (10)$$

In order to solve Eq. (10), following four variables are introduced:

$$z_1 = \delta, \quad (11)$$

$$z_2 = \frac{d\delta}{d\xi}, \quad (12)$$

$$z_3 = \frac{\dfrac{d^2\delta}{d\xi^2}}{\left\{1+\left(\dfrac{d\delta}{d\xi}\right)^2\right\}^{3/2}} + \frac{A}{\sigma\delta^3}, \quad (13)$$

$$z_4 = \frac{\sigma}{3\mu_l}\delta^3\frac{d}{d\xi}\left(\frac{\dfrac{d^2\delta}{d\xi^2}}{\left\{1+\left(\dfrac{d\delta}{d\xi}\right)^2\right\}^{3/2}} + \frac{A}{\sigma\delta^3}\right), \quad (14)$$

where variables z_1, z_2, z_3 and z_4 correspond to film thickness, film inclination, capillary pressure and flow rate, respectively. Then Eq. (10) can be rewritten as a system of four first order differential equations as follows:

$$\frac{dz_1}{d\xi} = z_2, \tag{15}$$

$$\frac{dz_2}{d\xi} = \left(z_3 - \frac{A}{\sigma z_1^3}\right)\left(1+z_2^2\right)^{3/2}, \tag{16}$$

$$\frac{dz_3}{d\xi} = \frac{3\mu_l}{\sigma}\frac{z_4}{z_1^3}, \tag{17}$$

$$\frac{dz_4}{d\xi} = \frac{T_{sat} - T_w + \dfrac{T_{sat}\sigma}{h_{fg}\rho_l} z_3}{\rho_l h_{fg}\left(\dfrac{\delta}{\lambda_l} + \dfrac{T_{sat}\sqrt{2\pi R_g T_{sat}}}{h_{fg}^2 \rho_v}\dfrac{2-f}{2f}\right)}. \tag{18}$$

This set of equations is integrated by fourth order Runge-Kutta method. The boundary conditions are shown in Fig. 4. At the macro and micro boundary, the film thickness z_{1in} , and z_{3in} ($=p_c/\sigma$) are set as

$$z_{1in} = \delta_{in}, \tag{19}$$

$$z_{3in} \approx K = 1/R_{in} = 1/R_{macro}(x). \tag{20}$$

The boundary film thickness δ_{in}, which determines the location of the micro-macro boundary, can be chosen arbitrarily. It is confirmed that the choice of δ_{in} does not affect the total heat transfer rate. The liquid film inclination angle z_{2in} and flow rate z_{4in} at the macro-micro boundary are chosen by iteration so that both film slope z_{2end} and flow rate z_{4end} become zero at the micro and adsorbed film boundary, i.e.

$$z_{2end} = 0, \tag{21}$$

$$z_{4end} = 0. \tag{22}$$

Macro Region Model

Then, the micro region model is combined with the macro region model. The schematic view of the flow along the groove is shown in Fig. 5. The shape of liquid-vapor interface in the macro region is assumed to be a circular arc. This

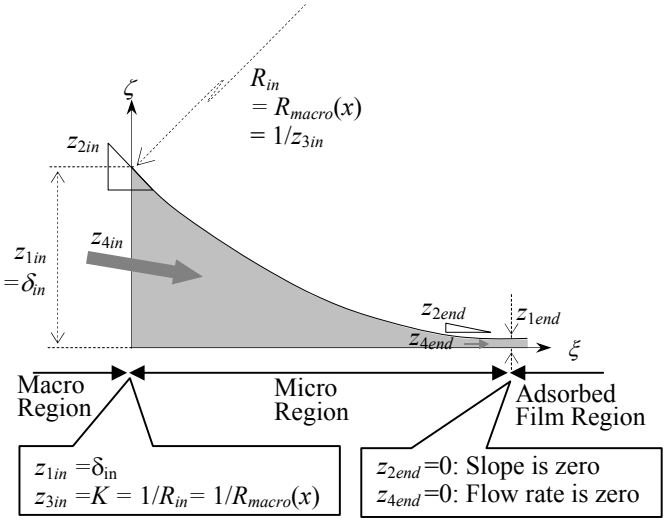

Fig. 4 Boundary conditions for the micro region

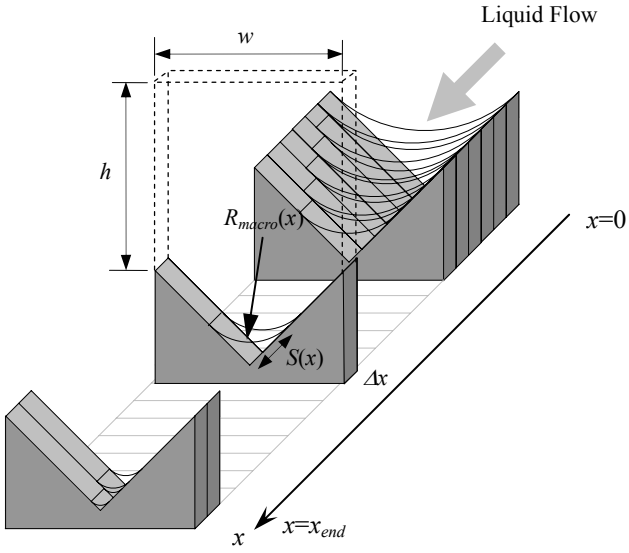

Fig. 5 Schematic view of the flow inside the groove

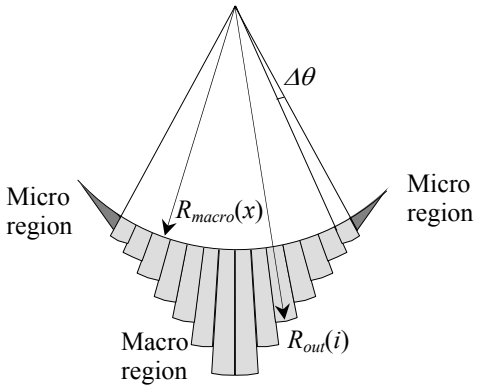

Fig. 6 Macro region modeling

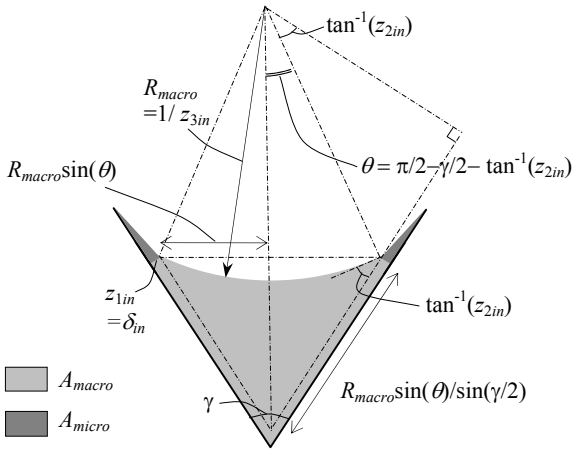

Fig. 7 Cross section of the triangular groove

curvature radius R_{macro} is used as the boundary condition for the micro region calculation at each cross section of the groove. In case of evaporators used in vapor compression cycles, liquid film on the wall is pushed with the vapor flow by the pressure gradient along the channel. Assuming large Froude number, gravity is also ignored in the macro region model. In principle, the film thickness is determined by the balance of streamwise pressure gradient and the shear stress in both fluids. However, it requires time consuming numerical procedures to capture the liquid-vapor interface. In the present study, the position of liquid-vapor interface is directly obtained from the Smith's[9] equation which predicts void fraction β from given quality χ;

$$\beta = \left(1 + \frac{\rho_v}{\rho_l}\left(\frac{1-\chi}{\chi}\right)\left(0.4 + 0.6\sqrt{\frac{\frac{\rho_v}{\rho_l} + 0.4\frac{1-\chi}{\chi}}{1 + 0.4\frac{1-\chi}{\chi}}} \right) \right)^{-1} . \qquad (23)$$

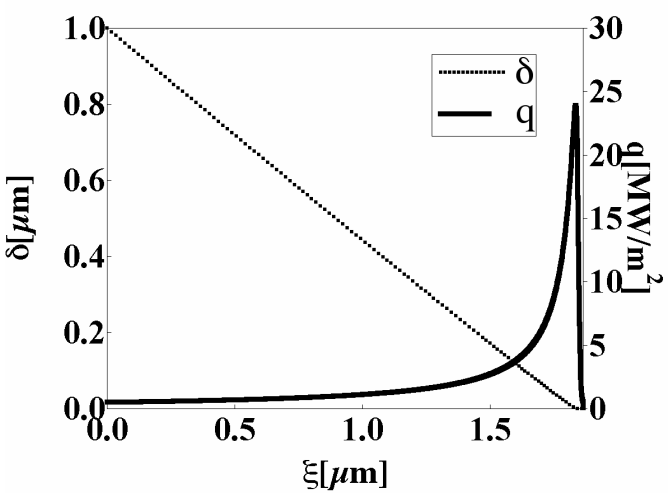

Fig. 8 Predicted local heat transfer coefficient and film thickness in the micro region

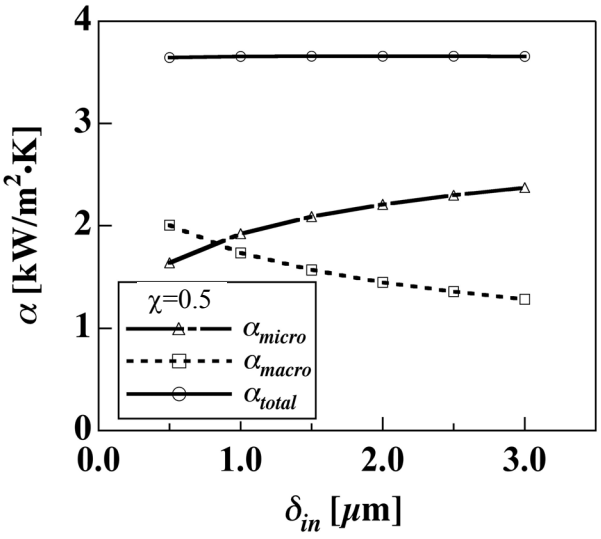

Fig. 9 Effect of film thickness δ_{in} at macro-micro boundary

This simple equation is originally derived for smooth pipe flows. In addition, Eq. (23) is independent on flow rate. However, Eq. (23) is known to give fairly good void fraction predictions for micro-fin tubes. And most thankfully, the film thickness can be obtained explicitly without solving a system of equations. This is a very attractive advantage from an engineering point of view. Thus, this simple approach is adopted in this study as a first order approximation.

The macro region is divided into concentric strips as shown in Fig. 6. The amount of heat transferred from each strip is calculated assuming one dimensional radial heat conduction, i.e.

$$\Delta Q = \frac{\lambda \cdot \Delta\theta}{\ln\left(R_{out}(i)\right)/\left(R_{macro}(x)\right)}\left(T_{sat} - T_w\right). \qquad (24)$$

The total macro region is divided into 200 strips in this study.

The simulation starts at x=0 where the tip of the micro region touches the crest of the groove, and ends where micro regions from both sides meet each other at the center of the groove as shown in Fig. 5. Once quality χ is known at any streamwise position x, the micro region model is calculated with an assumed curvature $R_{macro}(x)$. The value of curvature $R_{macro}(x)$ is modified iteratively until the calculated liquid area (A_{macro}+A_{micro}) shown in Fig. 7 satisfies the void fraction given from Eq.(23). With converged $R_{macro}(x)$, the total amount of liquid evaporated $\dot{g}_l(x)$ at position x is known from the sum of micro and macro region results. Thus, we can know the liquid flow rate $\dot{G}_l(x+\Delta x)$ (also quality) at the next position $x+\Delta x$ from Eq. (25). This procedure is continued until the liquid flow is dried out.

$$\dot{G}_l\left(x+\Delta x\right) = \dot{G}_l\left(x\right) - \dot{g}_l\left(x\right)\Delta x . \qquad (25)$$

Preliminary Evaluation of the Model

Figure 8 shows the predicted film thickness and heat flux profile in the micro region for HFC134a with T_w=253.15K and T_{sat}=248.15K. The groove width is w=0.9mm and the channel height is h=1.6mm. As the film thickness δ decreases, the

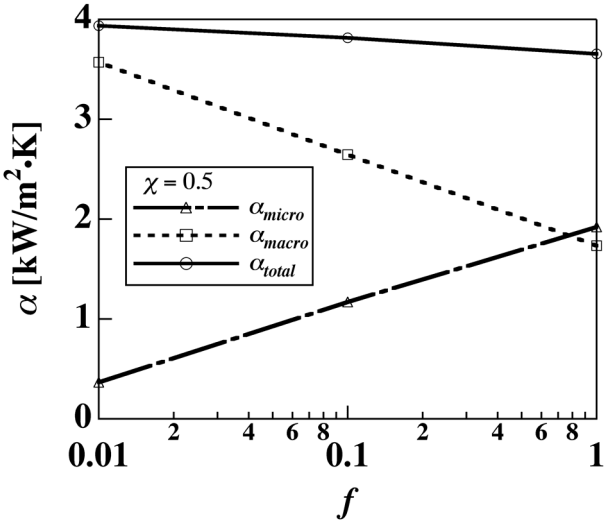

Fig. 10 Effect of accommodation coefficient f

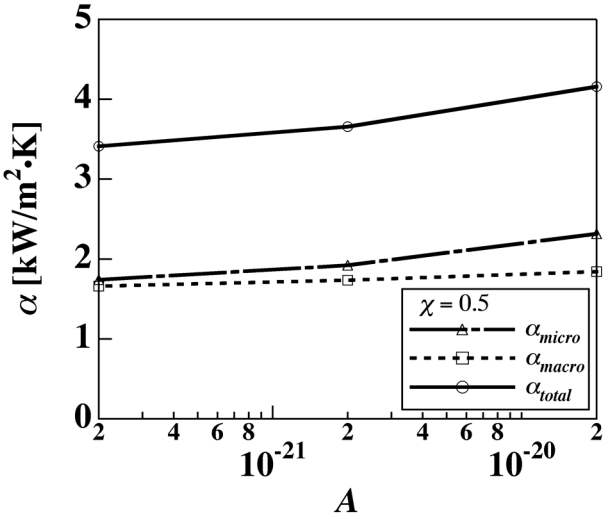

Fig. 11 Effect of dispersion constant A

thermal resistance of liquid film is reduced and thus the heat flux increases. However, as the liquid film gets much thinner, the capillary pressure p_c increases dramatically due to the disjoining pressure effect. This reduces the equilibrium vapor pressure at the interface which is the driving force of evaporation. Extremely high heat flux ($\dot{q}_{peak} > 20\,\mathrm{MW/m^2}$) is obtained at a very narrow area of the interline region, even for HFC134a which has relatively low thermal conductivity compared to water or ammonia. The film thickness is less than 100nm at the interline region.

The liquid film thickness at the location of macro-micro boundary, δ_{in}, can be chosen arbitrary as noted earlier. Figure 9 shows the predicted heat transfer coefficient for different boundary film thickness δ_{in}. Projected area of the groove is used for the definition of the heat flux, and the groove shape is equilateral triangle. The micro, macro and total heat transfer coefficients are defined as follows:

$$\alpha_{total} = \alpha_{micro} + \alpha_{macro} = \frac{\Delta Q_{micro}}{w \cdot \Delta x \cdot \Delta T} + \frac{\Delta Q_{macro}}{w \cdot \Delta x \cdot \Delta T}. \quad (26)$$

Although the ratio of micro to macro contributions varies with δ_{in}, the total heat transfer coefficient remains nearly constant. It is confirmed that the total heat transfer prediction is not affected by the location of micro macro boundary. Thus, the film thickness boundary value was fixed as δ_{in}= 1μm in this study.

Figures 10 and 11 show the effects of accommodation coefficient f and dispersion constant A on the predicted total heat transfer coefficient. As it can be seen from the figures, the total heat transfer coefficient is quite robust against wide variations of f and A. It is obvious that the accommodation coefficient f has large influence on the prediction near the contact line in the micro region. However, small f makes the liquid film inclination (dδ/dξ) much more moderate in the micro region. And this makes the effective thin film region longer in the macro region. It should be emphasized that this

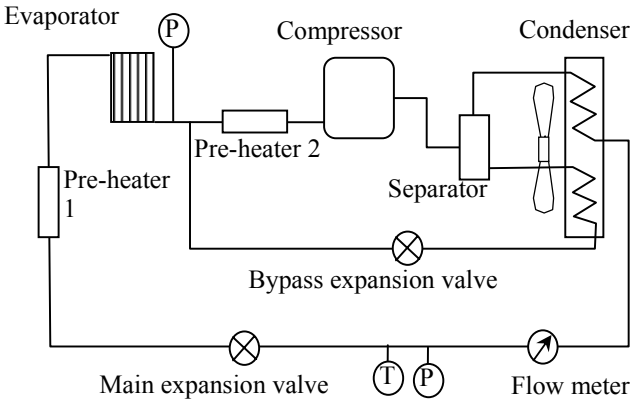

Fig. 12 Experimental setup

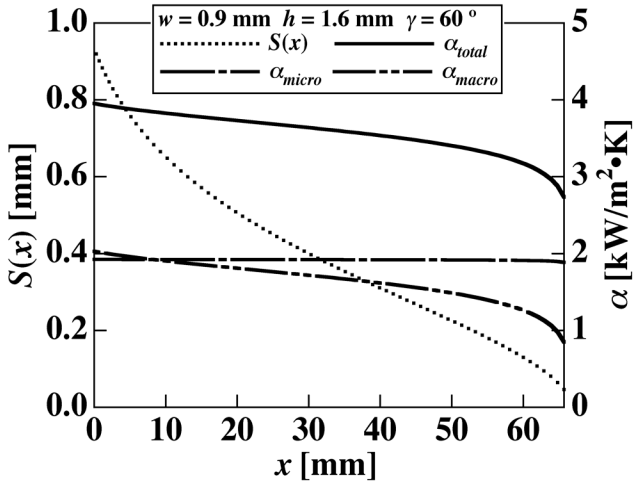

Fig. 13 Wet area width $S(x)$ and local heat transfer coefficient.

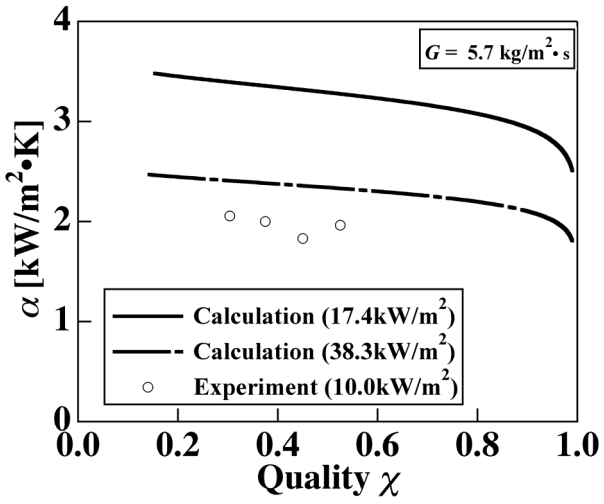

Fig. 14 Heat transfer coefficient against quality.

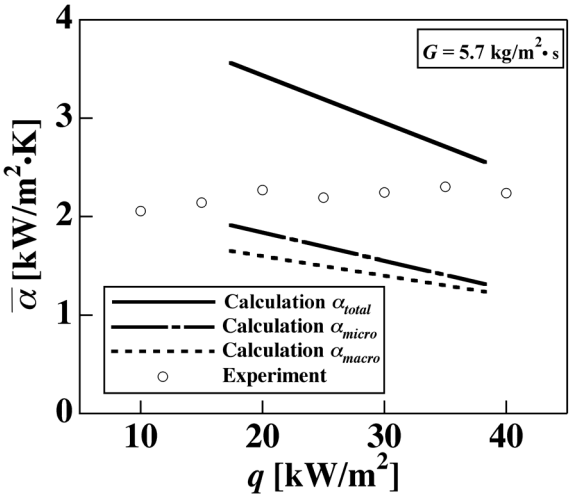

Fig. 15 Average heat transfer coefficient against heat flux

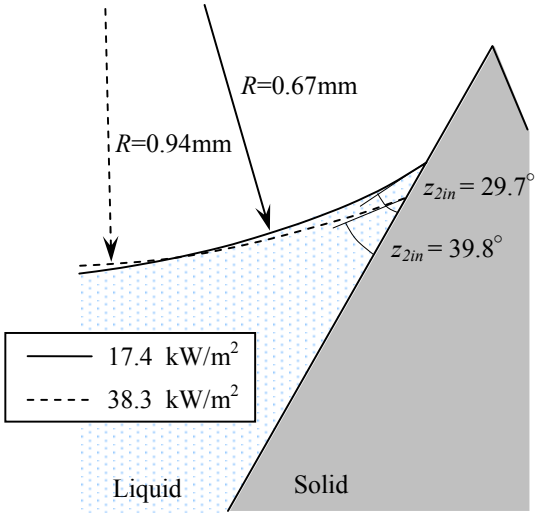

Fig. 16 Predicted liquid-vapor interface profile

robustness of the predicted total heat transfer coefficient against these microscopic parameters is a very desirable feature as an engineering design tool. Thus, $f = 1$ and $A = 2.0 \times 10^{-21}$ J are used as reference values in this study.

EXPERIMENTAL VERIFICATION

The schematic of the HFC134a experimental loop is shown in Fig. 12. Main and bypass expansion valves are controlled to get required flow rate at the evaporator test section. The size of the flat plate evaporator is 25mm (width) × 40mm (length). The width of the micro-groove is 0.9mm, and the shape is equilateral triangle (γ=60deg). Averaged wall temperature from 9 K-type thermocouples and the saturated temperature from the pressure gauge were used for the heat transfer coefficient calculations.

Figure 13 shows the predicted wet area width $S(x)$ (see Fig. 5 for its definition) and local heat transfer coefficient against flow direction. The macro region heat transfer coefficient and wet area width $S(x)$ decrease along the flow direction. On the other hand, the micro region heat transfer coefficient remains nearly constant. Thus, the decrease of the total heat transfer coefficient is due to the degraded heat transfer in the macro region.

Figure 14 shows the heat transfer coefficient against quality. Predicted heat transfer coefficient decreases as quality increases. Heat transfer coefficient is overpredicted nearly 70% when heat flux is small. For larger heat flux, prediction curve gets much closer to the experimental data even the absolute heat flux value is different. The average heat transfer coefficient is plotted against heat flux in Fig. 15. Calculated heat transfer coefficients for both micro and macro regions decrease as heat flux increases, while experimental result shows nearly no dependence on heat flux. No boiling bubbles were observed from the sight glass visualization. Thus, experimental data imply that the mechanism of micro groove evaporation has only weak dependence on the heat flux variation. Figure 16 shows the predicted liquid-vapor interface profiles in the macro region. The micro region is hardly recognizable when plotted in this size since its range is so small. Both inclination angle at the micro-macro boundary and the radius of curvature are larger for higher heat flux case (38.3kW/m^2). This change in the liquid-vapor interface profile deteriorates heat transfer for larger heat flux calculation. The agreement of calculation and experiment at high heat flux implies that the experimental liquid-vapor interface profile should be quite similar to that for high heat flux prediction curve, i.e. the broken line, shown in Fig. 16. Furthermore, this experimental liquid-vapor interface profile should remain nearly unchanged regardless of heat flux. It is considered that the difference between experiment and prediction can be attributed to the error in predicting the liquid-vapor interface profile. More elaborate modeling of liquid-vapor interface profile will be necessary for vapor compression cycle micro-grooved evaporators.

CONCLUSIONS

A micro-grooved flat plate evaporator is modeled and investigated by numerical analysis and experiment. The following conclusions are derived:

1. Variation in accommodation coefficient f and dispersion constant A has relatively small effect on total heat transfer coefficient prediction. This feature is really desirable for engineering applications.
2. Predicted heat transfer coefficient decreases as quality increases.
3. The predicted heat transfer coefficient shows strong dependence on heat flux, which is not the case with experimental data. It is considered that this difference can be attributed to the error in predicting the liquid-vapor interface profile.

ACKNOWLEDGMENTS

The authors thank Mr. Y. Mukasa for his help during constructing the experimental setup.

REFERENCES

[1] Wayner, P. C., Jr., 1999, "Intermolecular forces in phase-change heat transfer: 1998 Kern Award Review," AIChE J., **45**, pp. 2055-2068.

[2] Wayner, P. C., Jr., 1997, "Interfacial Forces and Phase Change in Thin Liquid Films," in Microscale Heat Transfer, Edited by C.L. Tien, F.W. Gerner, and A. Majumdar, Taylor & Francis, New York, Chapter 6, pp. 187-226.

[3] Wayner, P. C., Jr., Kao, Y. K. and LaCroix, L. V., 1976, "The interline heat-transfer coefficient of an evaporating wetting film," Int. J. Heat Mass Transfer, **19**, pp. 487-492.

[4] Wayner, P. C., Jr., 1982, "Adsorption and capillary condensation at the contact line in change of phase heat transfer, " Int. J. Heat Mass Transfer, **25**, pp. 707-713.

[5] Kamotani, Y., 1978, "Evaporator film coefficients of grooved heat pipes," Proc. 3rd Int. Heat Pipe Conf., Palo Alto, CA.

[6] Stephan, P. and Busse, C. A., 1992, "Analysis of the heat transfer coefficient of grooved heat pipe evaporator walls," Int. J. Heat Mass Transfer, **35**, pp.383-391.

[7] Ajaev, V. S. and Homsy, G. M., 2001, "Steady Vapor Bubbles in Rectangular Microchannels," J. Colloid Interface Sci., **240**, pp. 259-271.

[8] Hasebe, S., Shikazono, N. and Kasagi, N., 2004, "Modeling and Design of Micro Groove Falling Film Evaporators," Proc. 2nd Int. Conf. Microchannels & Minichannels, ICMM2004-2368, RIT, Rochester, NY.

[9] Smith, S. L., 1970, "Void fraction in two-phase flow: A correlation based upon an equal velocity head model," Heat and Fluid Flow, **1**, 1, p. 22.